Unsteady Transonic Flow Calculations for Realistic Aircraft Configurations

John T. Batina,* David A. Seidel,† Samuel R. Bland,‡ and Robert M. Bennett‡
NASA Langley Research Center, Hampton, Virginia

A transonic unsteady aerodynamic and aeroelasticity code called CAP-TSD has been developed for application to realistic aircraft configurations. The CAP-TSD code uses a time-accurate approximate factorization (AF) algorithm for solution of the unsteady transonic small-disturbance equation. The AF algorithm is very efficient for solution of steady and unsteady transonic flow problems. It can provide accurate solutions in only several hundred time steps, yielding a significant computational cost savings when compared to alternative methods. The new code can treat complete aircraft geometries with multiple lifting surfaces and bodies, including canard, wing, tail, control surfaces, launchers, pylons, fuselage, stores, and nacelles. Applications are presented for a series of four configurations of increasing complexity to demonstrate the wide range of geometrical applicability of CAP-TSD. These results are in good agreement with available experimental steady and unsteady pressure data. Calculations for the General Dynamics one-ninth-scale F-16C aircraft model are presented to demonstrate application to a realistic configuration. Unsteady results for the entire F-16C aircraft undergoing a rigid pitching motion illustrate the capability required to perform transonic unsteady aerodynamic and aeroelastic analyses for such configurations.

Nomenclature

c	= airfoil chord
c_r	= wing reference chord
C_p	= pressure coefficient
$\bar{C}_p$	= unsteady pressure coefficient normalized by oscillation amplitude
f	= position of horizontal lifting surface
g	= position of vertical lifting surface
k	= reduced frequency, $=\omega c_r/2U$
M	= freestream Mach number
t	= time, nondimensionalized by U/c_r
U	= freestream speed
x,y,z	= nondimensional physical coordinates in the streamwise, spanwise, and vertical directions, respectively
α	= angle of attack
β	= yaw angle
γ	= ratio of specific heats
δ	= control surface deflection angle
$\Delta\bar{C}_p$	= unsteady lifting pressure coefficient normalized by oscillation amplitude
Δt	= nondimensional time step
$\bar{\eta}$	= fractional semispan along exposed planform
Λ	= leading-edge sweep angle
ϕ	= disturbance velocity potential
ω	= angular frequency

Subscripts

b	= body
c	= canard
f	= fuselage
t	= tail
w	= wing
0	= mean value
1	= dynamic value

Presented as Paper 87-0850 at the AIAA/ASME/ASCE/AHS 28th Structures, Structural Dynamics and Materials Conference, Monterey, CA, April 6–8, 1987; received March 23, 1987; revision received Feb. 8, 1988. This paper is declared a work of the U.S. Government and is not subject to copyright protection in the United States.

*Research Scientist, Unsteady Aerodynamics Branch, Structural Dynamics Division. Senior Member AIAA.

†Research Engineer, Unsteady Aerodynamics Branch, Structural Dynamics Division. Member AIAA.

‡Senior Research Engineer, Unsteady Aerodynamics Branch, Structural and Dynamics Division. Associate Fellow AIAA.

Introduction

At present, considerable research is being conducted to develop finite-difference computer codes for calculating transonic unsteady aerodynamics for aeroelastic applications.[1] These computer codes are being developed to provide accurate methods of calculating unsteady airloads for the prediction of aeroelastic phenomena such as flutter and divergence. For example, the XTRAN3S[2] unsteady transonic small-disturbance (TSD) code was developed for transonic aeroelastic analyses of isolated planar wings. The code uses an alternating-direction implicit (ADI) finite-difference algorithm to calculate steady and unsteady transonic flows in a time-marching fashion. Several terms of the ADI algorithm are treated explicitly, however, which leads to a time-step restriction based on numerical stability considerations. Experience with the code has shown that, for applications to practical wings with moderate to high sweep and taper, very small time steps are required for the algorithm to be numerically stable.[3–6] This stability restriction typically results in thousands of time steps required to obtain converged steady solutions and thousands of steps per cycle of motion. Such solutions are computationally expensive, and thus, aeroelastic applications of XTRAN3S have generally been limited.

A new alternative algorithm based on approximate factorization (AF) was developed recently by Batina[7] for the time-accurate solution of the unsteady TSD equation. The AF algorithm involves a Newton linearization procedure coupled with an internal iteration technique. In Ref. 7, the AF algorithm was shown to be very robust and efficient for application to either steady or oscillatory transonic flows with subsonic or supersonic freestream conditions. The new algorithm can provide accurate solutions in only several hundred time steps, yielding a significant computational cost savings when compared to alternative methods. Furthermore, the AF algorithm is fully vectorizable, which results in an additional saving of computer resources. The Unsteady Aerodynamics

Branch at NASA Langley Research Center has subsequently developed a new computer code to fully exploit the superior stability characteristics and computational efficiency of the AF algorithm. The new code is called Computational Aero-elasticity Program-Transonic Small Disturbance (CAP-TSD). The code allows the analysis of complete aircraft configurations, including fuselages and multiple lifting surfaces. The development of the methodology for treating these components has been reported in Refs. 8 and 9. The CAP-TSD code also can treat pylons, stores, and nacelles using modeling similar to that of Boppe and Stern[10] and Shankar and Malmuth.[11] The CAP-TSD code, therefore, is capable of transonic unsteady aerodynamic and aeroelastic analysis of realistic aircraft configurations.

The purpose of this paper is to describe the development of the CAP-TSD computer code and to present unsteady transonic applications for realistic aircraft configurations involving multiple components. Specifically, the paper will 1) state the governing flowfield equations; 2) briefly reiterate the AF algorithm and solution procedure; 3) discuss the computational modeling of the wing, canard, tail, fuselage, pylons, stores, and nacelles in the context of the unsteady TSD equation; 4) introduce the CAP-TSD computer code; and 5) present results for several complex configurations that demonstrate the wide range of geometrical applicability of the new code. Finally, the results are validated by making comparisons with available experimental steady and unsteady data.

Governing Equations

In this section, the TSD equation, boundary conditions, and coordinate transformation are described briefly.

TSD Equation

The flow is assumed to be governed by the general-frequency modified TSD potential equation, which may be written in conservation law form as

$$\frac{\partial f_0}{\partial t}+\frac{\partial f_1}{\partial x}+\frac{\partial f_2}{\partial y}+\frac{\partial f_3}{\partial z}=0 \tag{1}$$

where

$$f_0=-A\phi_t-B\phi_x \tag{2a}$$

$$f_1=E\phi_x+F\phi_x^2+G\phi_y^2 \tag{2b}$$

$$f_2=\phi_y+H\phi_x\phi_y \tag{2c}$$

$$f_3=\phi_z \tag{2d}$$

The coefficients A, B, and E are defined as

$$A=M^2 \tag{3a}$$

$$B=2M^2 \tag{3b}$$

$$E=1-M^2 \tag{3c}$$

and the coefficients F, G, and H are defined as

$$F=-\tfrac{1}{2}(\gamma+1)M^2 \tag{4a}$$

$$G=\tfrac{1}{2}(\gamma-3)M^2 \tag{4b}$$

$$H=-(\gamma-1)M^2 \tag{4c}$$

Boundary Conditions

The conditions imposed on the outer boundary of the computational region are similar to the characteristic or "nonreflecting" boundary conditions reported by Whitlow.[12] The conditions employed here are given by

Upstream:

$$\phi=0 \tag{5a}$$

Downstream:

$$\frac{1}{2}\left(\frac{-B}{C}+\frac{D}{\sqrt{C}}\right)\phi_t+\phi_x=0 \tag{5b}$$

Above:

$$\frac{D}{2}\phi_t+\phi_z=0 \tag{5c}$$

Below:

$$\frac{D}{2}\phi_t-\phi_z=0 \tag{5d}$$

Right spanwise:

$$\frac{D}{2}\phi_t+\phi_y=0 \tag{5e}$$

Left spanwise:

$$\frac{D}{2}\phi_t-\phi_y=0 \text{ (full-span modeling)} \tag{5f}$$

Symmetry plane:

$$\phi_y=0 \text{ (half-span modeling)} \tag{5g}$$

where

$$C=E+2F\phi_x$$

$$D=\sqrt{4A+B^2/C}$$

Note that, when marching to steady state, the time derivatives in Eqs. (5b–f) vanish, resulting in simple Neumann boundary conditions. Thus, in this initial application study, the time derivatives have been neglected.

The horizontal lifting surfaces (canard/wing/horizontal tail/launcher) are modeled by imposing the following boundary conditions:

Flow tangency:

$$\phi_z^{\pm}=f_x^{\pm}+f_t \tag{6a}$$

Trailing wake:

$$[\phi_z]=0 \tag{6b}$$

$$[\phi_x+\phi_t]=0 \tag{6c}$$

where the brackets indicate the jump in the indicated quantity across the wake. The flow-tangency condition is imposed along the mean plane of the respective lifting surface. In Eq. (6a), the plus and minus superscripts indicate the upper and lower surfaces of the mean plane, respectively. The wakes are assumed to be flat and horizontal. The numerical implementation of Eqs. (6) allows for coplanar as well as noncoplanar combinations of canard, wing, horizontal tail, and launchers.

The vertical lifting surfaces (pylon/vertical tail) are modeled by imposing the following boundary conditions:

Flow tangency:

$$\phi_y^{\pm}=g_x^{\pm}+g_t \tag{7a}$$

Trailing wake:

$$[\phi_y] = 0 \tag{7b}$$

$$[\phi_x + \phi_t] = 0 \tag{7c}$$

where the brackets again indicate the jump in the indicated quantity across the wake. The flow-tangency condition is imposed along the vertical (x-z) mean plane of the respective lifting surface. In Eq. (7a), the plus and minus superscripts indicate the right and left surfaces of the mean plane, respectively. Flat vertical wakes are assumed for the pylons and vertical tail.

Bodies such as the fuselage, stores, and nacelles are treated as follows. For a body at angle of attack α_b and at yaw angle β_b, the flow-tangency boundary condition may be written as

$$N_t + N_x(1 + \phi_x) + N_y(\phi_y + \beta_b) + N_z(\phi_z + \alpha_b) = 0 \tag{8}$$

where $N(x,y,z,t) = 0$ defines the body surface. Computationally, bodies are modeled by applying simplified boundary conditions on a prismatic surface rather than on the true surface.[10,11] The method is consistent with the small-disturbance approximation and treats bodies with sufficient accuracy to obtain the correct global effect on the flowfield without the use of special grids or complicated coordinate transformations. As such, the approximations to the flow-tangency boundary condition [Eq. (8)] imposed on the prismatic surface are as follows:

Upstream face:

$$\phi_x = V_{\text{inlet}} - 1 \tag{9a}$$

Downstream face:

$$\phi_x = V_{\text{exit}} - 1 \tag{9b}$$

Left/right faces:

$$\phi_y = -C_t\left(\frac{N_x}{N_y} + \frac{N_t}{N_y}\right) - C_a\beta_b \tag{9c}$$

Top/bottom faces:

$$\phi_z = -C_t\left(\frac{N_x}{N_z} + \frac{N_t}{N_z}\right) - C_a\alpha_b \tag{9d}$$

where V_{inlet} and V_{exit} are the inlet and exit flow velocities, respectively, specified in the case of a nacelle as derived in Ref. 10. The parameters C_t and C_a are thickness and angle-of-attack corrections, respectively, derived using slender-body theory to account for the spatial differences between true and prismatic body surfaces.

The simplified body boundary conditions [Eqs. (9)] are analogous to the lifting-surface flow-tangency boundary conditions, which are imposed on the mean plane of the lifting surface rather than on the true surface. This method has been shown to be accurate for steady transonic applications for configurations with a fuselage, stores, and flow-through nacelles.[10] The body boundary conditions presented herein are extensions of those reported in Ref. 10 to allow analysis of unsteady transonic cases. Unsteady calculations for a wing/fuselage configuration were reported in Ref. 9, using similar body modeling.

Coordinate Transformation

The finite-difference grids in both the physical and computational domains are contained within rectangular boundaries and conform to the leading and trailing edges of the horizontal lifting surfaces. Regions in the physical domain are mapped into rectangular regions in the computational domain using a shearing transformation. For simplicity, no shearing is performed in the vertical direction so that pylons and vertical tails are approximated by rectangular surfaces.

Approximate Factorization Algorithm

An approximate factorization algorithm was developed to solve the modified TSD equation [Eq. (1)] and associated boundary conditions [Eqs. (5–7), (9)]. The algorithm consists of a Newton linearization procedure coupled with an internal iteration technique. For unsteady flow calculations, the solution procedure involves two steps: First, a time-linearization step is performed to determine an estimate of the potential field. Second, internal iterations are performed to minimize linearization and factorization errors. Specifically, the TSD equation [Eq. (1)] is written in general form as

$$R(\phi^{n+1}) = 0 \tag{10}$$

where ϕ^{n+1} represents the unknown potential field at time level $(n+1)$. The solution to Eq. (10) is then given by the Newton linearization of Eq. (10) about ϕ^*

$$R(\phi^*) + \left(\frac{\partial R}{\partial \phi}\right)_{\phi=\phi^*} \Delta\phi = 0 \tag{11}$$

In Eq. (11), ϕ^* is the currently available value of ϕ^{n+1} and $\Delta\phi = \phi^{n+1} - \phi^*$. During convergence of the iteration procedure, $\Delta\phi$ will approach zero so that the solution will be given by $\phi^{n+1} = \phi^*$. In general, only one or two iterations are required to achieve acceptable convergence.

The AF algorithm is formulated by first approximating the time derivative terms (ϕ_{tt} and ϕ_{xt} terms) by second-order-accurate finite-difference formulas. The TSD equation is rewritten by substituting $\phi = \phi^* + \Delta\phi$ and neglecting squares of derivatives of $\Delta\phi$, which is equivalent to applying Eq. (11) term by term. The resulting equation is then rearranged and the left-hand side is approximately factored into a triple product of operators, yielding

$$L_\xi L_\eta L_\zeta \, \Delta\phi = -R(\phi^*,\phi^n,\phi^{n-1},\phi^{n-2}) \tag{12}$$

where the operators L_ξ, L_η, and L_ζ, and the right-hand side R were derived in Ref. 7. Equation (12) is solved using three sweeps through the grid by sequentially applying the operators as

ξ sweep:

$$L_\xi \, \Delta\bar{\phi} = -R \tag{13a}$$

η sweep:

$$L_\eta \, \Delta\bar{\bar{\phi}} = \Delta\bar{\phi} \tag{13b}$$

ζ sweep:

$$L_\zeta \, \Delta\phi = \Delta\bar{\bar{\phi}} \tag{13c}$$

For steady flow calculations, the time derivatives of the AF algorithm are implemented for variable time stepping to allow step-size cycling for convergence acceleration. In these calculations, the step size is cycled using a standard geometric sequence. Further details of the algorithm development and solution procedure may be found in Ref. 7.

CAP-TSD Code

The AF algorithm has been used as the basis of the CAP-TSD code for transonic unsteady aerodynamic and aeroelastic analysis of realistic aircraft configurations. The present capability has the option of half-span modeling [Eq. (5g)] for sym-

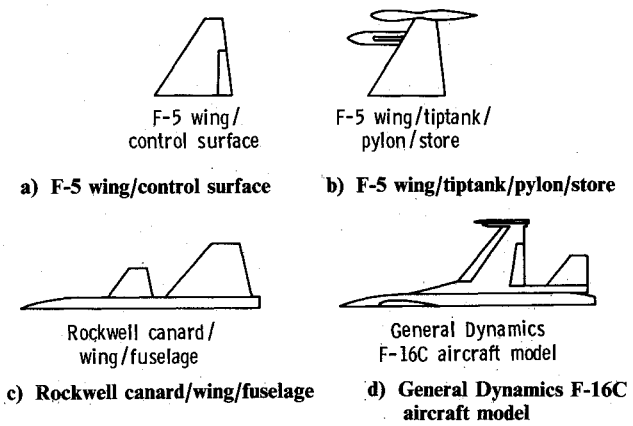

Fig. 1 Configurations for CAP-TSD analysis

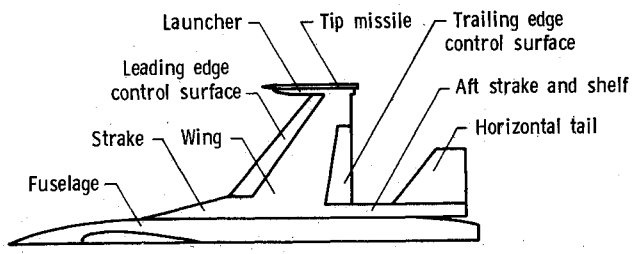

Fig. 2 CAP-TSD modeling of the General Dynamics one-ninth-scale F-16C aircraft model.

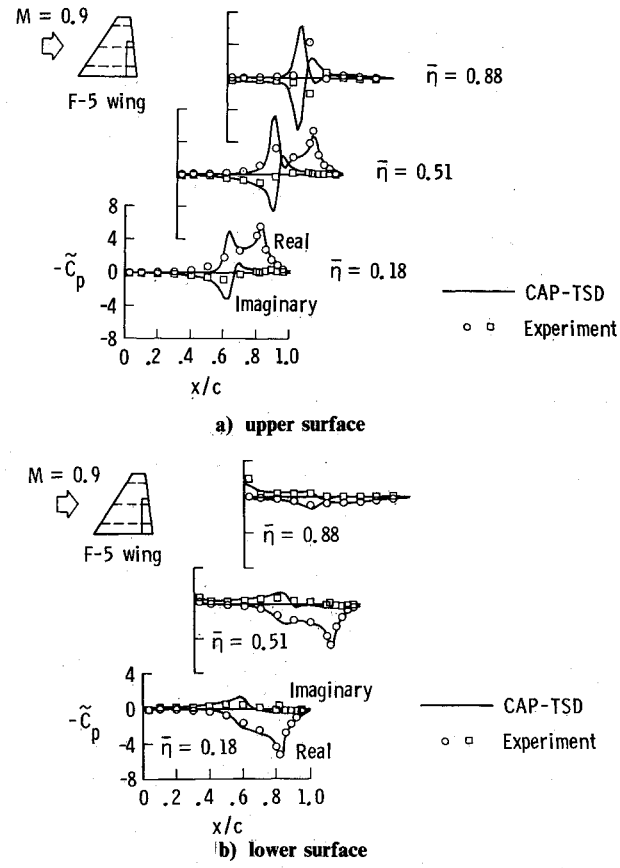

Fig. 3 Comparison between CAP-TSD and experimental unsteady pressure distributions on the F-5 wing due to control surface oscillation at $M = 0.9$, $\alpha_0 = 0$ deg, $\delta_1 = 0.471$ deg, and $k = 0.139$.

metric cases or full-span modeling [Eq. (5f)] to allow the treatment of antisymmetric mode shapes, fuselage yaw, or unsymmetric configurations such as an oblique wing or unsymmetric wing stores.

Computational efficiency is achieved through extensive vectorization of the AF algorithm as well as the CAP-TSD code in general. Since the L_ξ, L_η, and L_ζ operators of the AF algorithm contain only derivatives in their respective coordinate directions, all three sweeps of the solution procedure have been vectorized.

Results and Discussion

In this section, results are presented for a series of realistic aircraft configurations that demonstrate the efficiency, accuracy, and applicability of the CAP-TSD code. These configurations are described first, followed by a discussion of the corresponding calculations. The results are validated by making detailed comparisons with available steady and unsteady experimental pressure data. Further applications of CAP-TSD, including comparisons with experiment for supersonic freestream cases, are reported by Bennett et al.[14]

Configurations

Results are presented for the four configurations shown in Fig. 1. These configurations range in geometrical complexity from a simple wing with control surface to a realistic fighter geometry. The four configurations were selected to assess various geometry capabilities of CAP-TSD by making comparisons with the experimental pressure data of Refs. 15–20. A detailed description of each configuration is given in the following paragraphs.

The first configuration (Fig. 1a) is the F-5 wing with an inboard trailing-edge control surface.[15] The wing has a panel aspect ratio of 1.58, a leading-edge sweep angle of 31.9 deg, and a taper ratio of 0.28. The airfoil section of the F-5 wing is a modified NACA 65A004.8 airfoil, which has a drooped nose and is symmetric aft of 40% chord. The control surface has a constant percent-chord hingeline at 82% chord, inboard side edge at the wing root, and outboard side edge at 58% semispan. The calculations are compared with the experimental oscillatory pressure data from an F-5 wing model tested by Persoon et al.[15] Both subsonic and supersonic freestream cases are presented.

The second configuration (Fig. 1b) is the F-5 wing/tiptank/pylon/store geometry.[16] For this configuration, three components have been modeled in addition to the F-5 wing: 1) an area-ruled tiptank, which is an axisymmetric body of revolution with a fineness ratio (length/maximum diameter) of 10.88; 2) an underwing store, which is also an axisymmetric body of revolution with a fineness ratio of 7.04; and 3) a pylon, which connects the store to the lower surface of the wing at 77% semispan. The tiptank and store have angles of incidence relative to the wing zero angle of attack of −2.0 and −2.5 deg, respectively. A more detailed description of the F-5 wing/tiptank/pylon/store configuration is given in Refs. 16 and 17 along with the experimental pressure data. The calculations were performed for several combinations of F-5 components to investigate aerodynamic interference effects on steady and unsteady wing pressures.

For the first two configurations (Figs. 1a and 1b), unsteady as well as steady experimental pressure data are available for comparison with the CAP-TSD calculations. For the remaining configurations, however, only steady experimental pressure data exist to assess the accuracy of the calculated results. Unfortunately, there is a general lack of transonic unsteady pressure data for complex aircraft configurations, which is needed for code validation purposes.

The third configuration (Fig. 1c) is a canard/wing/fuselage model that was tested by Rockwell International.[18] The model consists of a swept-tapered canard and wing mounted to a relatively simple half-span fuselage. Each of the noncoplanar

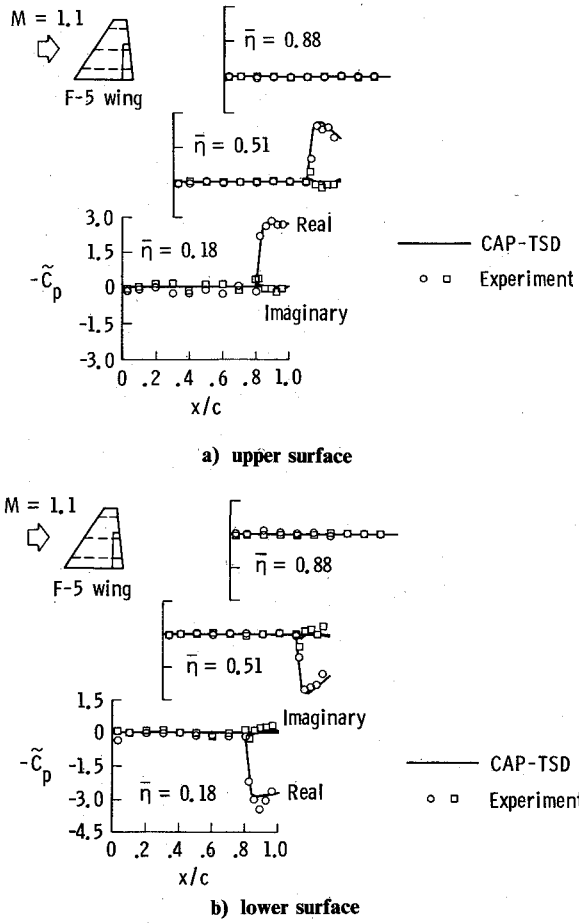

Fig. 4 Comparison between CAP-TSD and experimental unsteady pressure distributions on the F-5 wing due to control surface oscillation at $M = 1.1$, $\alpha_0 = 0$ deg, $\delta_1 = 0.45$ deg, and $k = 0.118$.

lifting surfaces has a panel (exposed) aspect ratio of approximately 1.0, a leading-edge sweep angle of 40 deg, a taper ratio slightly greater than 0.25, and a supercritical airfoil section. The wing also has 4 deg of incidence relative to the fuselage and 5 deg of parabolic twist washout. The Rockwell canard/wing/fuselage configuration is further described in Ref. 18 along with the experimental steady pressure data.

The fourth configuration (Fig. 1d) is the one-ninth-scale F-16C aircraft model, which was tested by General Dynamics.[19] Shown in Fig. 2 are the F-16C components that are modeled using CAP-TSD. The F-16C is modeled using four lifting surfaces and two bodies. The lifting surfaces include: 1) the wing with leading- and trailing-edge control surfaces; 2) the launcher; 3) a highly swept strake, aft strake, and shelf surface; and 4) the horizontal tail. The bodies include: 1) the tip missile and 2) the fuselage. Other salient features of the F-16C modeling include 3 deg linear twist washout for the wing, a leading-edge control surface hingeline that is straight but not of constant-percent chord, and a 10 deg anhedral for the horizontal tail. The rather detailed geometry description for the one-ninth-scale F-16C aircraft model was obtained from Ref. 19, and the experimental steady pressure data is tabulated in Ref. 20. Parallel calculations were also performed for the wing alone to investigate the effects of aerodynamic interference by making comparisons with the complete airplane results. These wing-alone calculations were performed for the outer wing panel only, with a plane of symmetry assumed at the wing root.

F-5 Wing/Control-Surface Results

Results were obtained for the F-5 wing/control surface configuration to assess the accuracy and efficiency of the CAP-TSD code for oscillatory control surface applications. In these

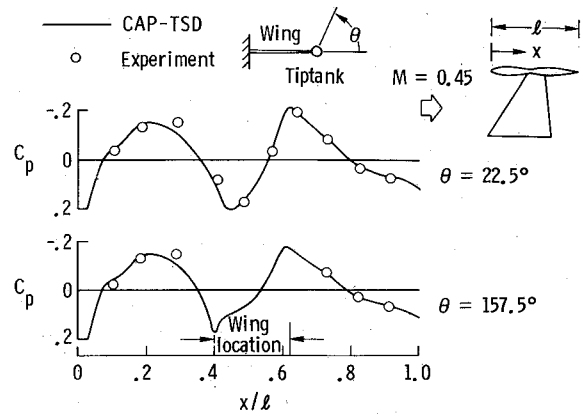

Fig. 5 Comparison between CAP-TSD and experimental steady pressure distributions on the tiptank of the F-5 wing/tiptank configuration at $M = 0.45$ and $\alpha_0 = 0$ deg.

calculations, two Mach number cases were selected. The first case, case 1 of Table 1, was chosen to have the same freestream conditions as investigated in Refs. 3, 4, and 7. In case 1, the freestream Mach number was 0.9, and both the mean angle of attack and mean control surface deflection angle were zero. The second case, case 2 of Table 1, was chosen to assess the performance of CAP-TSD for oscillatory control surface motion with supersonic freestream conditions. In case 2, the freestream Mach number was 1.1 and again the mean angle of attack and mean control surface deflection angle were both zero. In cases 1 and 2, both steady and unsteady results were obtained for comparison with the experimental data of Refs. 13 and 15. Steady pressure distributions for these cases were presented and compared with the experiment data in Ref. 7 and, therefore, are not repeated here. Unsteady pressure results for these cases are described in the following paragraphs.

Case 1

For case 1, unsteady results were obtained for the control surface oscillating with amplitude $\delta_1 = 0.471$ deg at a reduced frequency of $k = 0.139$. The calculations were performed using only 300 steps per cycle of motion, which corresponds to a step size of $\Delta t = 0.07354$. Three cycles of motion were computed to obtain a periodic solution. Unsteady pressure distributions along three span stations of the wing are plotted in Fig. 3 along with the experimental data. The unsteady pressure coefficients along the upper surface are shown in Fig. 3a; the unsteady pressure coefficients along the lower surface are shown in Fig. 3b. These coefficients are plotted as real and imaginary components corresponding to the in-phase and out-of-phase unsteady pressure distributions normalized by the amplitude of motion. As shown in Fig. 3a, there is a calculated shock pulse of moderate strength on the upper surface of the wing. The shock pulse is due to the motion of the upper-surface shock wave and is overpredicted in magnitude in comparison with the experimental data. This is generally what is expected from a conservative inviscid potential flow code. For cases such as this, the inclusion of the nonisentropic effects[21] and viscous effects[22] could be expected to improve the correlation between calculation and experiment. Overall, the CAP-TSD results generally agree well with the experimental data, especially in predicting the control surface pressures (Figs. 3a and 3b).

Case 2

For case 2, unsteady results were obtained for the control surface oscillating with amplitude $\delta_1 = 0.45$ deg at a reduced frequency of $k = 0.118$. Similar to case 1, the calculations also were performed using 300 steps per cycle of motion, which corresponds to a step size of $\Delta t = 0.08875$. Only two cycles of motion were required to obtain a periodic solution. Calculations for the third cycle of motion produced results that were

identical to the second cycle results, to plotting accuracy. This faster convergence is due to the lack of upstream signal propagation resulting from the supersonic nature of the flow. Figure 4 shows a comparison of CAP-TSD unsteady pressures with the experimental data. Upper-surface pressure distributions are shown in Fig. 4a; lower-surface pressure distributions are shown in Fig. 4b. The CAP-TSD results indicate that the pressures on the control surface are nearly in-phase with the motion since the imaginary components are very small in comparison to the real components. Also, the pressures are zero outside of the domain of influence of the control surface, which is expected for supersonic flow. The CAP-TSD results are in very good agreement with the experimental pressure data along both the upper (Fig. 4a) and lower (Fig. 4b) surfaces of the wing.

F-5 Wing/Tiptank/Pylon/Store Results

Results were obtained for the F-5 wing/tiptank/pylon/store configuration to assess the CAP-TSD modeling for multiple body geometries. In these calculations, one case was selected—case 3 of Table 1. For this case, results are presented for the F-5 wing/tiptank geometry both with and without the pylon and store included in the calculation. Comparisons of these results reveal interference effects on wing pressures. In case 3, the freestream Mach number was selected as $M = 0.45$ for direct comparison with the published subsonic experimental pressure data of Refs. 16 and 17. Both steady and unsteady results were obtained for the wing at zero mean angle of attack. The unsteady calculations were performed for the configuration pitching harmonically at a reduced frequency of $k = 0.147$. The configuration was forced to pitch about a line perpendicular to the root at 15% chord from the wing apex. The results were obtained using 300 steps per cycle of motion, which corresponds to a step size of $\Delta t = 0.07135$.

Case 3

For case 3, steady pressure distributions on the tiptank are presented first, to assess the accuracy of the CAP-TSD body modeling. As shown in Fig. 5, two sets of pressures are plotted corresponding to inboard ($\theta = 157.5$ deg) and outboard ($\theta = 22.5$ deg) longitudinal lines along the tiptank. These pressure distributions show expansions near the fore and aft maximum diameter locations as well as a compression near the area-ruled middle region. The calculated tiptank pressures are in very good agreement with the experimental data, which validates the CAP-TSD body modeling.

Steady pressure distributions on the wing at 72% semispan are presented in Fig. 6. Two sets of calculated and experimental results are plotted corresponding to the wing/tiptank configuration with and without the pylon/store included. As shown in the lower part of Fig. 6, inclusion of the pylon and store significantly increased (negatively) the lower-surface pressures from the wing leading edge to approximately 65% chord. The interference effect of the pylon and store on the wing lower-surface steady pressures is largest in the pylon location region, as expected. The effect on the upper-surface pressures is negligible, as shown in the upper part of Fig. 6. The calculated steady pressures for cases with and without the pylon/store compare very well with the experimental data.

Unsteady pressure distributions for case 3 are presented in Fig. 7. Two sets of calculated and experimental results are again plotted corresponding to the wing/tiptank configuration with and without the pylon/store. As shown in the upper part of Fig. 7, inclusion of the pylon and store increased the real component of the unsteady lifting pressure. The effect on the imaginary component is negligible. The CAP-TSD results are in good agreement with the experimental pressure data in predicting the aerodynamic interference effect of the pylon/store.

Rockwell Canard/Wing/Fuselage Results

Results were obtained for the Rockwell canard/wing/fuselage configuration to assess CAP-TSD for multiple lifting-surface and fuselage applications. In these calculations, one case

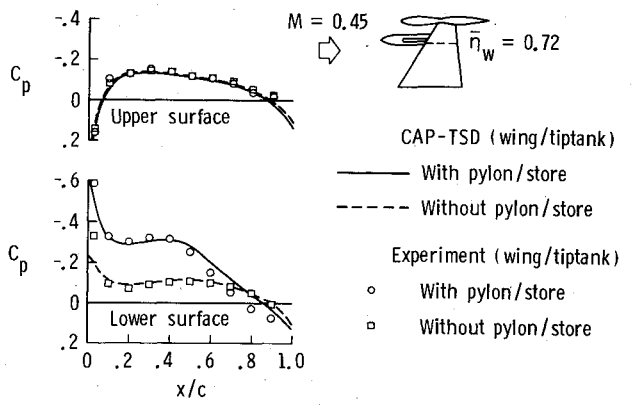

Fig. 6 Comparison between CAP-TSD and experimental steady pressure distributions on the wing of the F-5 wing/tiptank configuration both with and without pylon/store at $M = 0.45$ and $\alpha_0 = 0$ deg.

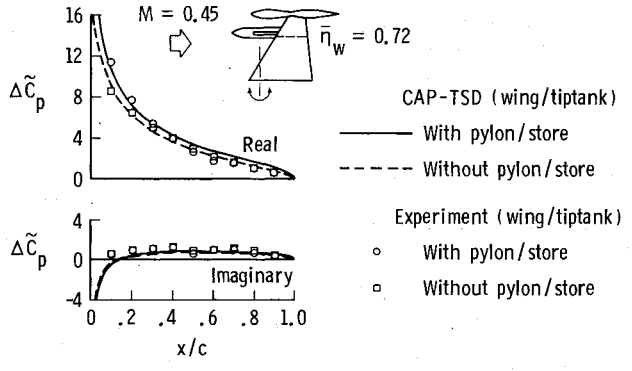

Fig. 7 Comparison between CAP-TSD and experimental unsteady pressure distributions on the wing of the F-5 wing/tiptank configuration both with and without pylon/store at $M = 0.45$, $\alpha_0 = 0$ deg, and $k = 0.147$.

Table 1 Cases for CAP-TSD analysis

Configuration	Case	M
F-5 wing/control surface	1	0.9
	2	1.1
F-5 wing/tiptank/pylon/store	3	0.45
Rockwell canard/wing/fuselage	4	0.8
General Dynamics F-16C aircraft model	5	0.9

was considered: case 4 of Table 1. In case 4, the freestream Mach number was $M = 0.8$ for comparison with the experimental steady pressure data of Ref. 18. The angle of attack for both the canard and wing was 2.05 deg. For the wing, this angle is added to the incidence and twist so that the root and tip are effectively at 6.05 and 1.05 deg, respectively.

Case 4

For case 4, comparisons of CAP-TSD and experimental steady pressure distributions on the canard and wing are plotted in Fig. 8. Chordwise pressures along one span station of the canard and along three span stations of the wing were selected for comparison with the data. As shown in Fig. 8, the CAP-TSD pressures are in favorable agreement with the experimental data along both lifting surfaces. The small differences between calculation and experiment in the wing upper-surface trailing-edge region are due to flow separation. The overpredicted pressures along the lower surface of both the canard and

the wing, aft of approximately 85% chord, are due to viscous effects. Of course, flow separation and viscous effects are outside the scope of the present capability.

General Dynamics F-16C Aircraft Model Results

Results were obtained for the General Dynamics one-ninth-scale F-16C aircraft model to demonstrate application of CAP-TSD to a realistic configuration. In these calculations, one case was considered, case 5 of Table 1, which corresponds to $M = 0.9$. Additional results for $M = 0.85$ and 1.1 were reported in Ref. 23. The CAP-TSD results were obtained for the F-16C aircraft at 2.38 deg angle of attack and with the leading-edge control surface of the wing deflected upwards 2 deg for comparison with the experimental steady pressure data of Ref. 20. These steady pressure comparisons are made to assess the accuracy of CAP-TSD for complete airplane applications. There are no unsteady experimental data to validate the CAP-TSD code for time-accurate F-16C calculations. Nonetheless, an unsteady calculation was performed for case 5 to demonstrate the time-accurate capability. For simplicity, the calculation was performed for a rigid pitching motion, where the entire F-16C aircraft was forced to oscillate about the model moment reference axis at a reduced frequency of $k = 0.1$. The oscillation amplitude was chosen as $\alpha_1 = 0.5$ deg, and 300 steps per cycle of motion were computed corresponding to $\Delta t = 0.1047$. Parallel results were also obtained for the wing alone to investigate the aerodynamic interference effects of the additional aircraft components on wing unsteady pressures.

For the F-16C configuration, all of the calculations were performed on a grid which conforms to the leading and trailing edges of the lifting surfaces, including the strake, and which contained 324,000 points. This grid included 160, 27, and 75 points in the streamwise, spanwise, and vertical directions, respectively. The grid was relatively easy to generate, even for such a complex configuration as the F-16C aircraft, since the sectional (x-z) grids are Cartesian. Also, the calculations required only about 0.88 CPU s/time step and 13 million words of memory on the CDC VPS-32 computer.

For case 5, steady pressure comparisons for the F-16C aircraft model are presented in Fig. 9 for three span stations of the wing and one span station of the tail. In this case ($M = 0.9$), there is a moderately strong shock wave on the upper surface of the wing, and the CAP-TSD pressures again generally agree well with the experimental pressures. The shock is slightly overpredicted in strength and located slightly aft of the experimental location, which is expected from a conservative inviscid potential flow code. Similar to case 1, the inclusion of the nonisentropic effects and viscous effects could be expected to improve the correlation between calculation and experiment. For the tail, the flow is predominantly subcritical and the CAP-TSD pressures agree well with the experimental data.

Unsteady pressure distributions along the wing and tail upper surfaces are shown in Fig. 10 for the entire F-16C aircraft undergoing a rigid pitching motion. These unsteady pressure results are presented at the same span stations as the steady-state results (Fig. 9). Two sets of calculated pressures are compared corresponding to complete airplane and wing-alone modeling. As shown in Fig. 10, there is a relatively large shock pulse in the real part of the wing upper-surface pressures. This shock pulse is of larger magnitude and is located further downstream in the complete airplane model. These features are attributed to a stronger steady-state shock on the upper surface of the wing produced by the accelerated flow about the fuselage and the launcher/tip missile. The unsteady pressures near the leading edge of the wing are also generally of larger magnitude for the complete airplane. For the tail, the unsteady pressures are relatively small in comparison with the wing pressures and, thus, were plotted on an expanded scale. The tail is located considerably aft of the pitch axis and, thus, its motion is plunge dominated, which results in smaller airloads for the low value

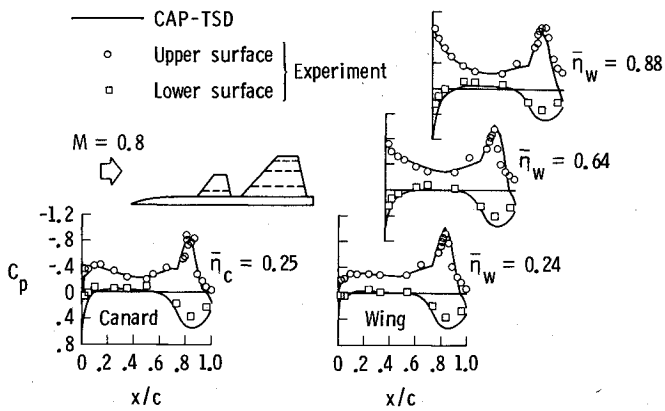

Fig. 8 Comparison between CAP-TSD and experimental steady pressure distributions on the canard and wing of the Rockwell canard/wing/fuselage configuration at $M = 0.8$, $\alpha_c = \alpha_w = 2$ deg, and $\alpha_f = 0$ deg.

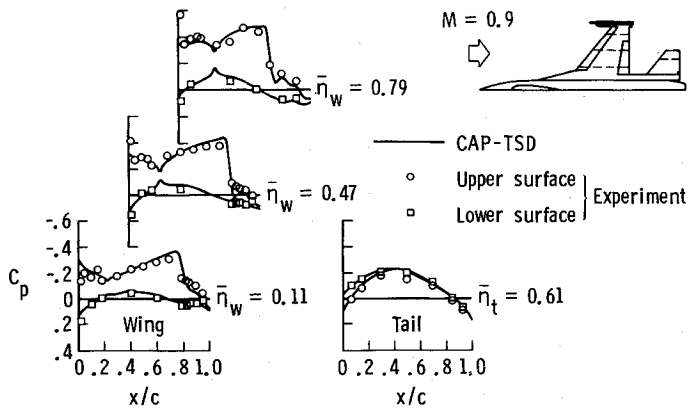

Fig. 9 Comparison between CAP-TSD and experimental steady pressure distributions on the wing and tail of the F-16C aircraft model at $M = 0.9$ and $\alpha_0 = 2.38$ deg.

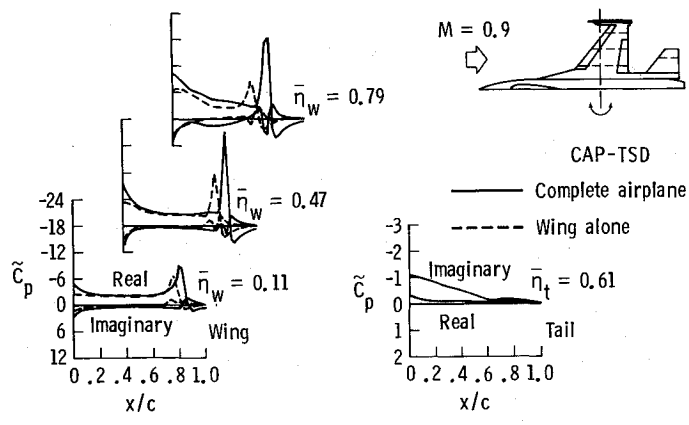

Fig. 10 CAP-TSD unsteady pressure distributions on the wing and tail upper surface of the F-16C aircraft model due to complete airplane rigid pitching at $M = 0.9$, $\alpha_0 = 2.38$ deg, $\alpha_1 = 0.5$ deg, and $k = 0.1$.

of k considered. Furthermore, these pressures are nearly 90 deg out of phase with the aircraft motion since the real components are small compared to the imaginary components. The complete airplane and wing-alone results on the wing lower surface show much smaller differences than the results for the wing upper surface due to the subcritical nature of the flow (not shown).

Concluding Remarks

A transonic unsteady aerodynamic and aeroelasticity code called CAP-TSD has been developed for application to realistic aircraft configurations. The new code now permits the calculation of unsteady flows about complete aircraft configurations for aeroelastic analysis in the flutter-critical transonic speed range. The CAP-TSD code uses a time-accurate approximate factorization (AF) algorithm for solution of the unsteady transonic small-disturbance equation. The AF algorithm has been shown to be very efficient for steady or unsteady transonic flow problems. It can provide accurate solutions in only several hundred time steps, yielding a significant computational cost savings when compared to alternative methods. For reasons of practicality and affordability, an efficient algorithm and a fast computer code are requirements for realistic aircraft applications.

Results were presented for several complex aircraft configurations that demonstrated the geometrical applicability of CAP-TSD. The code can treat configurations with arbitrary combinations of lifting surfaces and bodies, including canard, wing, tail, control surfaces, tip lauchers, pylons, fuselage, stores, and nacelles. Most of the cases presented are steady-state calculations for comparison with available experimental data.

Calculations presented for the F-5 wing with an inboard trailing-edge oscillating control surface demonstrated the accuracy and efficiency of CAP-TSD for unsteady flows with subsonic and supersonic freestream conditions. These results compared well with the experimental data. Steady pressure distributions obtained for the Rockwell canard/wing/fuselage were also in good agreement with the experimental pressure data. The favorable comparisons thus verified the CAP-TSD coding for multiple lifting-surface and fuselage geometries and also demonstrated the accuracy of the program for such applications. Steady and unsteady calculations for the F-5 wing with a tiptank and underwing pylon/store further demonstrated CAP-TSD geometry capabilities. Comparisons of pressure distributions for combinations of F-5 components revealed aerodynamic interference effects on wing pressures. These calculated results were in good agreement with the experimental pressure data, which further assessed CAP-TSD for multiple-component applications with mutual interference effects.

Finally, results were presented for the General Dynamics one-ninth-scale F-16C aircraft model, which demonstrated application to a realistic configuration. The F-16C components modeled with CAP-TSD include: the wing with leading- and trailing-edge control surfaces; a highly swept strake, aft strake, and shelf surface; the tip launcher and missile; the horizontal tail; and the fuselage. Steady results at transonic conditions compared well with the experimental data. Unsteady results for the entire F-16C aircraft undergoing a rigid pitching motion were presented. Comparisons with parallel wing-alone results revealed aerodynamic interference effects of the additional aircraft components on wing unsteady pressures. These effects emphasize the importance of including all components in the calculation. The CAP-TSD code thus provides the capability of modeling complete aircraft configurations for realistic transonic and supersonic unsteady aerodynamic and aeroelastic analyses.

References

[1]Edwards, J. W. and Thomas, J. L., "Computational Methods for Unsteady Transonic Flows," AIAA Paper 87-0107, Jan. 1987.

[2]Borland, C. J. and Rizzetta, D. P., "Nonlinear Transonic Flutter Analysis," *AIAA Journal*, Vol. 20, Nov. 1982, pp. 1606–1615.

[3]Guruswamy, G. P. and Goorjian, P. M., "Efficient Algorithm for Unsteady Transonic Aerodynamics of Low-Aspect-Ratio Wings," *Journal of Aircraft*, Vol. 20, March 1985, pp. 193–199.

[4]Borland, C. J. and Sotomayer, W. A., "An Algorithm for Unsteady Transonic Flow About Tapered Wings," AIAA Paper 84-1567, June 1984.

[5]Bennett, R. M., Wynne, E. C., and Mabey, D. G., "Calculation of Transonic Steady and Oscillatory Pressures on a Low Aspect Ratio Model and Comparison with Experiment," Paper 85-17, Second International Symposium on Aeroelasticity and Structural Dynamics, Technical Univ. of Aachen, FRG, April 1985.

[6]Guruswamy, G. P., Goorjian, P. M., Ide, H., and Miller, G. D., "Transonic Aeroelastic Analysis of the B-1 Wing," *Journal of Aircraft*, Vol. 23, July 1986, pp. 547–553.

[7]Batina, J. T., "Efficient Algorithm for Solution of the Unsteady Transonic Small-Disturbance Equation," *Journal of Aircraft*, Vol. 25, July 1988, pp. 598–605.

[8]Batina, J. T., "Unsteady Transonic Flow Calculations for Interfering Lifting Surface Configurations," *Journal of Aircraft*, Vol. 23, May 1986, pp. 422–430.

[9]Batina, J. T., "Unsteady Transonic Flow Calculations for Wing-Fuselage Configurations," *Journal of Aircraft*, Vol. 23, Dec. 1986, pp. 897–903.

[10]Boppe, C. W. and Stern, M. A., "Simulated Transonic Flows for Aircraft with Nacelles, Pylons, and Winglets," AIAA Paper 80-0130, Jan. 1980.

[11]Shankar, V. and Malmuth, N., "Computational and Simplified Analytical Treatment of Transonic Wing/Fuselage/Pylon/Store Interactions," *Journal of Aircraft*, Vol. 18, Aug. 1981, pp. 631–637.

[12]Whitlow, W., Jr., "Characteristic Boundary Conditions for Three Dimensional Transonic Unsteady Aerodynamics," NASA TM 86292, Oct. 1984.

[13]Tijdeman, H. et al., "Transonic Wind Tunnel Tests on an Oscillating Wing with External Stores," Air Force Flight Dynamics Lab., TR-78-194, Dec. 1978.

[14]Bennett, R. M., Bland, S. R., Batina, J. T., Gibbons, M. D., and Mabey, D. G., "Calculation of Steady and Unsteady Pressures on Wings at Supersonic Speeds with a Transonic Small-Disturbance Code," AIAA Paper 87-0851, April 1987.

[15]Persoon, A. J., Roos, R., and Schippers, P., "Transonic and Low Supersonic Wind-Tunnel Tests on a Wing with Inboard Control Surface," Air Force Wright Aeronautical Lab., TR-80-3146, Dec. 1980.

[16]Renirie, L., "Analysis of Measured Aerodynamic Loads on an Oscillating Wing-Store Combination in Subsonic Flow," NLR MP 74026 U, Sept. 1974.

[17]Bennekers, B., Roos, R., and Zwann, R. J., "Calculation of Aerodynamic Loads on Oscillating Wing/Store Combinations in Subsonic Flow," NLR MP 74028 U, Sept. 1974.

[18]Stewart, V. R., "Evaluation of a Propulsive Wing/Canard Concept at Subsonic and Supersonic Speeds, Rockwell International, Rept. NR82H-85, Feb. 1983.

[19]Fox, M. C. and Feldman, C. S., "Model and Test Information Report, 1/9-scale F-16C and F-16D Force and Loads Model," General Dynamics, Rept. 16PR2179, Jan. 1982.

[20]Feldman, C. S., "Wind Tunnel Data Report, 1/9-Scale F-16C Pressure Loads Test," General Dynamics, Rept. 16PR2252, July 1982.

[21]Gibbons, M. D., Whitlow, W., Jr., and Williams, M. H., "Nonisentropic Unsteady Three Dimensional Small Disturbance Potential Theory, AIAA Paper 86-0863, May 1986.

[22]Howlett, J. T., "Efficient Self-Consistent Viscous-Inviscid Solutions for Unsteady Transonic Flow," *Journal of Aircraft*, Vol. 24, Nov. 1987, pp. 737–744.

[23]Batina, J. T., Seidel, D. A., Bland, S. R., and Bennett, R. M., "Unsteady Transonic Flow Calculations for Realistic Aircraft Configurations," AIAA Paper 87-0850, April 1987.